

Chapter 5

Inelastic Neutron Scattering on Polymer Electrolytes for Lithium-Ion Batteries

Hua-Gen Peng,¹ Madhusudan Tyagi,^{2,3} Kirt A. Page,¹
and Christopher L. Soles^{1,*}

¹Polymers Division, National Institute of Standards and Technology,
Gaithersburg, MD 20899

²NIST Center for Neutron Research, National Institute of Standards and
Technology, Gaithersburg, MD 20899

³Dept. of Materials Science and Engineering, University of Maryland,
College Park, MD 20742

*csoles@nist.gov

The relationship between ion transport and polymer dynamics is central to the pursuit of solid polymer electrolytes for lithium batteries. This understanding is critical to achieve solid polymer electrolyte systems of sufficiently high ion conductivities. Solid polymer electrolytes are highly attractive from the perspective of their mechanical properties and low flammability compared to current electrolytes, however their ionic conductivities are typically an order of magnitude lower than the liquid electrolytes that are used today in commercial Li⁺ ion battery systems. Here we introduce inelastic neutron scattering (INS) as a tool to quantify the coupling between the local dynamics in the polymer electrolyte with the ion mobility through this ion transport media. INS techniques are well suited for this task as they are primarily sensitive to the dynamics of the hydrogen rich polymer electrolyte and not the Li⁺ ions themselves. This is complimentary to dielectric or impedance measurements which in battery systems loaded with ionic charge carriers are primarily sensitive to the dynamics of these ions; the impedance contribution from the organic electrolyte is usually overshadowed by the ions. The combination of INS and dielectric measurements provides the opportunity to directly correlate ion dynamics with the dynamics of the host

electrolyte to better understand this complicated ion transport process. In this chapter we briefly introduce some of the basic INS techniques that can be used for these studies and review the current literature focused on understanding the dynamics in organic and polymer electrolytes for Li⁺ ion batteries.

Introduction

Lithium-ion rechargeable batteries are widely used in portable electronics and are quickly becoming critical power sources for current and future electric vehicles, primarily due to their high energy density, light weight, and high operational voltage (*1*). Current lithium-ion batteries utilize organic liquid electrolytes such as propylene carbonate or ethylene carbonate that come with several shortcomings which limit their wide-spread usage in large load applications such as electric vehicles and stationary power. These liabilities are safety related and include electrolyte leakage, decomposition, flammability, and a propensity to develop catastrophic short circuits from lithium dendrites (*2, 3*). Solid polymer electrolyte (SPE) rechargeable lithium batteries offer several potential advantages over current battery technologies based on liquid electrolytes. Easy containment of the solid electrolyte allows for more latitude in designing the battery shape, an ability to handle higher energy densities, and reduced environmental hazards and flammability (*1, 2*). However, these potential advantages have not been fully realized after decades of research due to the generally low conductivities of SPEs compared to liquid electrolytes.

Poly(ethylene oxide) (PEO) is the most prominent example of a SPE due to its ability to solvate and transport lithium-ions. However, PEO is semi-crystalline with a high degree of crystallinity (> 70%) and the Li-ion transport is limited primarily to the minor domains of the mobile amorphous phase. The result is that unmodified PEO has a low Li-ion conductivity (10^{-6} S/cm) below its melting temperature ($T_m = \sim 65$ °C) (*4, 5*). This is far below the target of 10^{-3} S/cm that is required for current battery applications (*3, 6, 7*). There are several strategies to suppress crystallization of PEO and improve conductivity. One approach has been to decrease the crystalline fraction through the incorporation of propylene oxide (PO) units into the PEO backbone (*5*). While this prevents crystallization, the Li-ion conductivity of these polymers is not substantially improved. It is thought that the nonpolar propyl groups also reduces the solubility of Li-ions in the polyelectrolyte and thus the mobile charge carriers (*3*). An analogous approach has been to graft oligo(ethylene glycol) units to other flexible polymers, resulting in comb-branched architectures that will solvate Li-ions (*3, 8, 9*). There have also been attempts to swell polyether polymers with small polar molecules, such as propylene carbonate and ethylene carbonate. While effective at improving conductivity, these gel-type systems still have safety issues related to the leakage of liquid additives (*5, 10*). Cross-linked and branched polymers have also been explored as polymer electrolytes (*11–13*), but their Li-ion conductivities remain well below the threshold of 10^{-3} S/cm. As a rule of thumb the ionic conductivity of typical SPEs with Li⁺ ions are approximately 10^{-4} S/cm, about an order of

magnitude lower than the organic liquid electrolytes that are used in current Li⁺ ion battery technologies. Dramatic increases in ionic conductivity are needed to realize SPE Li⁺ ion batteries. This is not an entirely unrealistic goal by any means. Beta alumina is a solid ceramic electrolyte that can conduct Na⁺ ions with mobilities on the order of 10⁻² S/cm (14). However, to get to this point with SPEs requires the understanding of Li⁺ ion conduction mechanism.

It is generally accepted that the Li⁺ ion conduction is regulated through cooperative motions of the polymer chain (5). The exact nature of this coupling on the molecular level is still not completely understood. It is generally acknowledged that the hopping rate of the charge carriers is directly influenced by fast local motions of the chain segments. In this chapter we describe inelastic neutron scattering (INS) as a powerful tool to quantify dynamics on the time and length scales that are relevant for ion transport. INS has long been used to investigate the dynamics in polymeric, ceramic, and biological materials (15–18). The application expanded to polymer electrolytes about a decade and half ago. The first part of this chapter will focus on describing the basics of several different INS measurement techniques while the second half will focus on examples of applying INS measurements to Li⁺ ion battery electrolytes. The primary objective of this chapter is to enlighten the battery field about INS and stimulate broader application of INS. However, the methodology is general and can be applied to a range of systems where ions or small molecules must pass through a dynamically active membrane. Other relevant examples include fuel cell membranes, flow batteries, and reverse osmosis membranes for water filtration.

Inelastic Neutron Scattering

INS is a versatile and powerful tool for quantifying the dynamics in biological and soft materials. The basis of the technique is illustrated schematically in Figure 1. A beam of neutrons with a narrow, well-defined energy distribution is focused onto the sample of interest. Different INS spectrometers vary in their ability to monochromate the energies of the incident neutron, but typically (for the sake of illustration) the beam can be focused into a narrow Gaussian energy distribution centered on E_0 . The solid lines in Figure 1 indicate such a distribution. When the incident beam of neutrons collides with the atomic nuclei in the sample, the strong nuclear interactions scatter the neutrons in various directions. The energy distribution of the scattered neutrons changes in comparison to the initial distribution. Some of the neutrons gain or lose energy through the dynamic interactions with the sample while others are scattered elastically, with no energy exchange. Figure 1 shows that there are generically two types of INS events. The left panel depicts scattering from a vibrating atomic nucleus, the motion confined within a well-defined potential energy minimum. The well-defined minimum leads to a distinct peak in the scattered energies. The shift in scattered peak from the incident energy indicates the energy of the excitation and this type of scattering is typically referred to as pure inelastic scattering. The second type of scattering is depicted in the right panel of Figure 1 where there is a diffusive motion of the atomic nucleus from one location to another. This results in a

diffuse broadening of the incident energy distribution. In the right panel of Figure 1 the narrow Gaussian distribution broadens into something more resembling a Lorentzian (as an example). Conventionally this diffuse broadening is referred to as quasielastic scattering (QES), although it is technically still a form of INS. By understanding the energy exchange between the sample and the neutrons, it is possible to perceive the atomic or molecular dynamics in the sample.

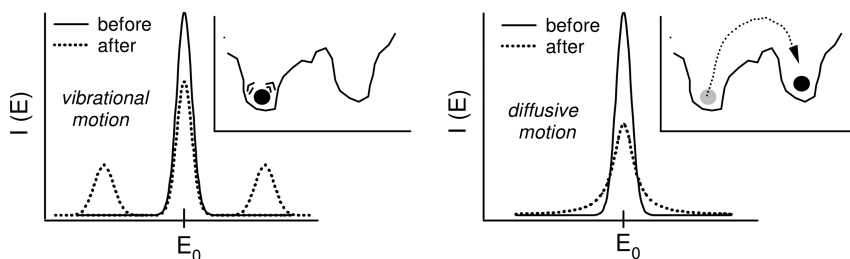


Figure 1. A cartoon depicting the two general types of energy exchange between a sample and a neutron for vibrational (left) and relaxational (right) molecular motions.

This type of inelastic scattering to measure sample dynamics is used with both light and X-rays in addition to neutrons. However, there are several attributes that make neutron scattering ideal for quantifying dynamics in biological and/or soft materials. First, the wavelength of most neutrons is between 1 Å and 10 Å, commensurate with many of the interatomic or intermolecular distances in soft organic materials. The length scale of the motions over which a motion is probed is given by the scattering vector $Q = 4\pi\sin(\theta)/\lambda$. In this expression θ is scattering angle and λ is the neutron wavelength. With most INS instruments it is reasonable to probe scattering over a range of angles that encompass a reciprocal space domain of $0.2 \text{ \AA}^{-1} < Q < 2.0 \text{ \AA}^{-1}$. In real space that corresponds to length scales approximately 3 Å to 30 Å, well suited for characterizing local atomic and molecular motions in organic materials.

The second property of neutrons that makes them useful for measuring polymer dynamics is their energy. Most cold neutrons that have passed through a liquid He moderator have energies that are on the order of a few meVs, on the same order of magnitude as the activation energies for many of the solid state excitations, molecular relaxations, and dynamic processes that occur in polymeric and soft materials. This means that when a neutron gains or loses energy from a dynamic interaction with the sample, the change in the energy of the neutron is usually a significant fraction of the initial neutron energy. This means that it is relatively easy to ascertain if a neutron has changed energy upon scattering. In contrast, X-rays in most scattering experiments have energies on the order of a

few keV. This is at least 6 to 7 orders of magnitude greater than the typical solid and liquid state excitations that occur in most polymeric materials. Most X-rays scatter or penetrate polymers with very little change in the energy of the incident beam. To discriminate a meV change in the energy of a keV source requires extremely sensitive energy discrimination.

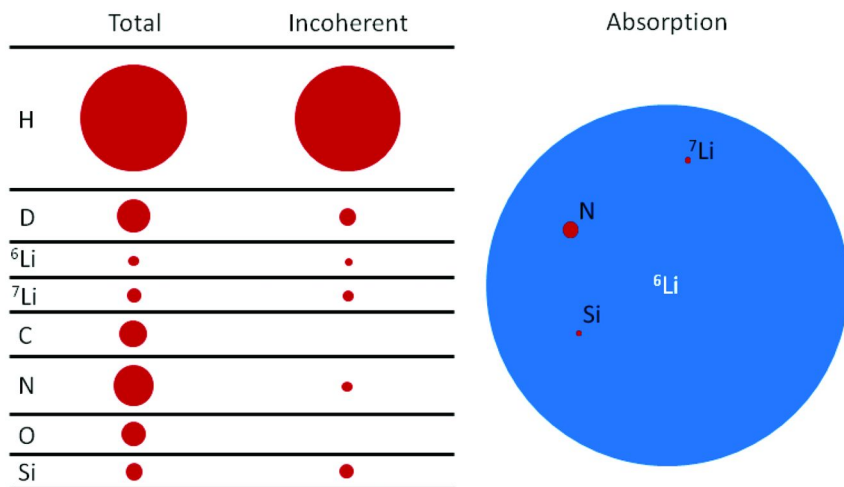


Figure 2. A series of circles are shown for different elements that are commonly encountered in the electrolyte media for Li-ion batteries. The areas of the circles have been scaled to reflect the differences in their neutron cross-sections, including the total scattering, incoherent scattering, and neutron absorption cross-sections.

The final reason why neutrons are ideal for measuring dynamics in organic and polymeric materials, especially in battery systems, is related to the scattering cross-section of the elements commonly present in these components, such as C, O, N, Li, H, and Si. With X-rays the scattering is dominated by the heavier elements and the scattering cross-section increases with atomic number. However, the strength of the nuclear interactions changes in more of a random manner with atomic number. Fortunately, hydrogen has the largest incoherent scattering cross-section of all the elements for neutron scattering. This is shown graphically in Figure 2 where the area of the circle represents the magnitude of the different scattering cross-sections; H rich moieties will dominate an inelastic scattering experiment. This is quite useful because H dynamics are difficult to quantify with complimentary optical and X-ray scattering techniques that are often insensitive to the lighter elements. The utility of neutron scattering is further enhanced by the fact that the isotopic switch from hydrogen (H) to deuterium (D) greatly

reduces this massive scattering cross-section. From a chemistry point of view, the switch from H to D is usually trivial in terms of modifying the physical properties, meaning that powerful isotopic labeling schemes can be devised. By selectively replacing certain H with D, one can study the dynamics isolated to a certain species or selected side group or moiety of the macromolecule. A similar analogy could be made with the radioisotope labeling schemes often used in nuclear magnetic resonance (NMR) measurements.

It is also notable that Li, in either its natural state of ${}^6\text{Li}$ or in its readily available isotope of ${}^7\text{Li}$, does not have an appreciable incoherent scattering cross-section compared to H. This means that inelastic neutron scattering is naturally more sensitive to the dynamics of the hydrogenous electrolyte material than the mobile Li^+ ions that carry the charge. This is in contrast to dielectric or impedance spectroscopy in which the signal is dominated by the strong charges on the ionic species. Impedance spectroscopy is well-suited to characterize dynamics of the charged ionic species. As the ions typically are inorganic or lack H, inelastic neutron scattering is more sensitive to the dynamics in the polymer organic electrolyte. As we discuss later, these measurements turn out to be very complimentary. Additionally, there is a very big difference between the neutron absorption cross sections between ${}^6\text{Li}$ and ${}^7\text{Li}$. Although we do not discuss it here, this becomes extremely useful in adapting neutron reflectivity and depth profiling techniques to quantify Li distributions across an interface. These methods are discussed in greater detail in other chapters of this book.

The combination of a large scattering cross-section with incident beam energies that are comparable to the intrinsic excitation energies means that hydrogen rich organic and polymeric materials scatter neutrons with large changes in the energy of the incident neutron beam. Using spectrometers that are sensitive to these energy changes, it is easy to quantify the energy gain/loss from the scattered neutrons. From energy and angular dependencies of the scattered neutrons, it is possible to determine the time and length scales of the dynamic processes in polymers. This is the fundamental basis for inelastic neutron scattering.

The neutron scattering cross-section of an element can be broken into its coherent and incoherent components (there is also an absorption cross-section which is unrelated to scattering which we will not address here). The cross-section reflects the number of neutrons scattered from a unit volume divided by the flux of the incident neutron beam. For coherent scattering events, there is a spatial correlation between the scattering from different nuclei of the same type. These spatial correlations allow us to determine the Van Hove or the pair-pair correlation function, i.e., the spatial correlations between the different atoms. For incoherent scattering events this spatial correlation is lost and there is no relation between scattering events between different pairs of atoms. However, the energy gained or lost by the scattered neutron is still perceivable. By converting the energy exchange into the time domain one can determine the Van Hove self-correlation function. This tells us that at a time, t (defined by the energy exchange), how far the nucleus has moved from its initial position at $t = 0$. From the energy and angular dependence of the incoherent scattering one can determine the time and length scale of the relaxations or other dynamic motions in a polymeric system.

Above, we mention that hydrogen has the largest scattering cross-section of all the elements. Its cross-section is nearly all incoherent; the coherent scattering from hydrogen is negligible. Figure 2 displays a series of circles whose areas are scaled proportionally to both the total and incoherent scattering cross-section of the nuclei they represent. From this representation it is apparent that inelastic neutron scattering is primarily sensitive to the dynamics of the hydrogen containing chemical groups or moieties. As most polymers are hydrocarbons, their incoherent scattering is very strong. Inelastic neutron scattering is one of the most direct methods to quantify the time and length scales of polymer dynamics.

The dynamic processes and relaxations that occur in polymers span a broad range of time and length scales. It is generally not possible to access the full phase space of time and length scales of these processes in a single inelastic neutron scattering experiment. Different types of experiments are sensitive to different regions of this phase space, as illustrated in Figure 3. The three primary techniques that have been utilized with respect to battery materials include neutron spin echo spectroscopy (NSE), backscattering spectroscopy (BS), and time-of-flight spectroscopy (TOF). The primary difference among the three techniques is the time and length scale of the dynamics probed. The NSE is sensitive to the slowest motions of the three spectrometers, perceiving dynamic processes on a time scale of 10^{-7} sec to 10^{-10} sec or dynamics in the micro- to nano-second range. To place the NSE technique in context, most solid state NMR instruments are sensitive to dynamic processes on the order of a microsecond and slower. As larger objects tend to move slower, NSE is also sensitive to the longer range motions; length scales on the order of 0.1 nm to 25 nm are common on NSE experiments. At these time and length scales, NSE can be used to monitor diffusive motions of polymer chains or large scale collective motions that span across tens to hundreds of atoms. By comparison, BS measurements are sensitive to slightly faster and shorter range motions. Most backscattering spectrometers are only sensitive to those motions faster than a nanosecond (slower motions appear as static or elastic scattering) at length scales that are comparable to most wide angle X-ray diffraction experiments. This spans molecular and atomic displacements nominally in the 1 Å to 30 Å range, which includes not just atomic vibrations but also some of the segmental motions. In polymers these often include side group motions, such as methyl rotations or crank shaft motions of chain segments. TOF spectrometers are sensitive to the fastest dynamics of the three instruments, perceiving dynamics on the order of picoseconds and faster over comparable length scales as in the BS instrument. At these time scales the dynamical processes probed in TOF experiments are typically atomic or molecular vibrations. Many of the same modes seen in infrared or Raman spectroscopy are also evidenced by TOF spectroscopy. Yet unlike infrared or Raman, there are no optical selection rules as to which modes are visible; the closest equivalent of would be the scattering cross section. In this respect, TOF can be regarded as more sensitive to the vibrational and high frequency relaxation processes of the hydrogenous moieties in the sample. To properly interpret experimental neutron scattering data for polymers under strong states of confinement, it is important to remain cognizant of the time and length scales of the motions that the spectrometer is sensitive to.

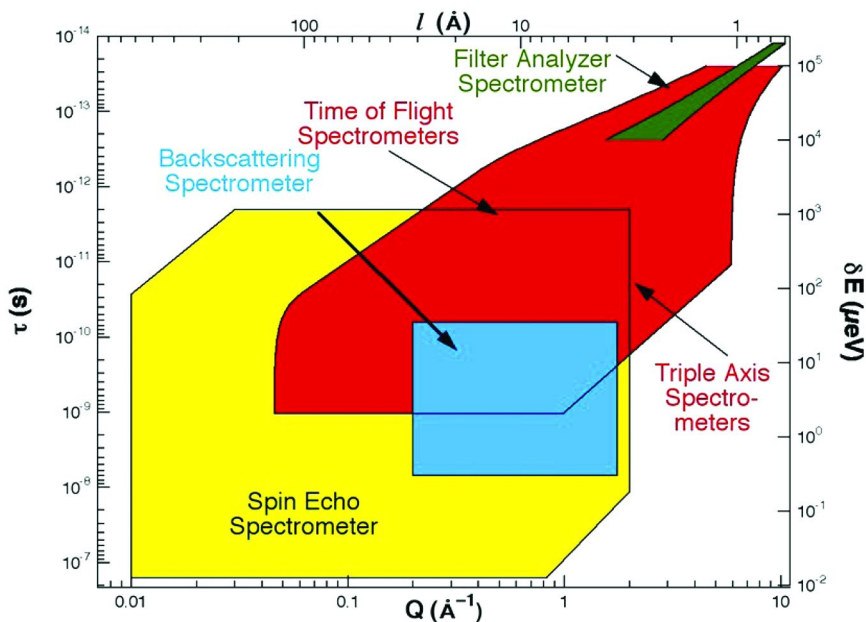


Figure 3. This figure maps out the length and energy scales that are accessible with the different types of inelastic neutron scattering techniques. In this chapter we have limited our discussion to the time of flight spectrometers, backscattering spectrometers, and spin echo spectrometers. Figure obtained from the NIST Center for Neutron Research Website (19).

Neutron Scattering Instrumentation

INS experiments require access to a neutron scattering facility. While there are only a handful of these in most major countries, access is often encouraged and most users find the facilities open to the scientific and research communities in general. The measurements described in this chapter put an emphasis on the NIST Center for Neutron Research (NCNR). The NCNR is a federally funded facility that is open to the general public. The user community at the NCNR spans academic, industrial, and government scientists from the United States and all over the world. Information about utilizing the NCNR facilities can be found through the NCNR's website (19). This chapter will mainly discuss the three types of INS spectrometers at the NCNR which were already mentioned above: the Time-of-Flight Spectrometer (TOF) (20), the High Flux Backscattering Spectrometer (HFBS) (21), and the Neutron Spin-Echo Spectrometer (NSE). Analogs of these are instruments are commonly found at most major neutron scattering facilities around the world, so the discussion is not limited to the NCNR. In the following section we briefly review the way in which these three instruments operate.

The TOF spectrometer is conceptually straightforward. It operates on the principal that when scattered neutrons gain energy, they speed up. Likewise, when

neutrons lose energy, they slow down. By measuring the time of flight of the scattered neutron across a fixed length from the sample to the detector, the energy of the scattered neutron can be determined. A schematic in Figure 3 depicts how a typical TOF spectrometer operates. The neutron beam enters a monochromator that only allows neutrons of a well-defined wavelength, and therefore a well-defined energy distribution, to pass through. This ideally mono-energetic beam of neutrons comes from a “chopper” that periodically releases pulses of neutrons onto the sample. The distance from the chopper to the sample and then from the sample to the detectors is accurately known for each TOF spectrometer. Since the energy or speed of the incident beam of neutrons is known (defined by the monochromator), it is straightforward to predict how long it should take a given pulse of neutrons to leave the chopper, scatter from the sample elastically, and then reach the detector. If the actual time of arrival at the detector is sooner than predicted, the neutrons have gained energy. If the time of arrival is later, the neutrons have lost energy through the scattering event. As Figure 4 shows, there are actually several detectors equidistant from the sample, spread out in a semicircle. This allows the dynamics to be probed over a large Q range, or range of different length scales.

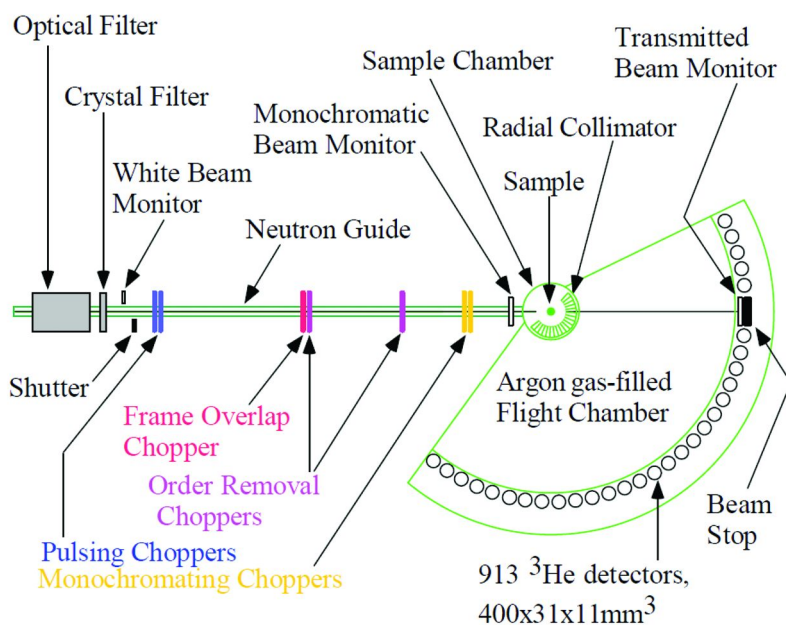


Figure 4. A schematic representation of the Disc Chopper Spectrometer time-of-flight inelastic neutron spectrometer available through the NCNR (19). The neutrons fly down the guide into the energy monochromator and then are periodically pulsed onto the sample at well-defined intervals. By precisely knowing the distance from the chopper to the sample and the flight path to the detector, one can quantify the neutron time-of-flight and thus the energy gained or lost in the scattering event.

Typically, the incident energy distribution of such instruments, described by the full-width at half maximum (FWHM), is on the order of 10 to 100 μeV . This energy resolution means that the instrument is sensitive to motions faster than approximately 5 GHz. A better energy resolution would mean that slower motions could be detected. As a scale of reference, these motions are a few orders of magnitude faster than the KHz to MHz processes that can be probed by NMR. It may also be useful to think of these energy resolutions in terms of wave numbers. The Disc Chopper TOF spectrometer at NCNR can see modes higher in energy than approximately 0.1 cm^{-1} ($1 \text{ meV} = 8 \text{ cm}^{-1}$).

The NIST HFBS spectrometer is a fixed final energy spectrometer. The details of this spectrometer are described in Figure 5. A beam of neutrons travels down the converging guide and bounces backwards off of a phase space transformation (PST) chopper, toward monochromator. The phase space chopper allows only those neutrons with a wavelength of 6.271 \AA to pass onto the the Si- $\langle 111 \rangle$ monochromator. The monochromator reflects these 6.271 \AA neutrons (in yellow) back towards the phase space chopper and into the sample (in red). When the neutrons hit the sample, they scatter at different angles into the Debye-Scherrer ring of reflectors. The Debye-Scherrer rings composed of Si-111 also reflect only those neutrons with a wavelength of 6.271 \AA back towards a bank of ^3He detectors that resides just behind and slightly above the sample. Given that all of the neutron optics in this system is designed for 6.271 \AA neutrons, only elastically scattered neutrons reach the detectors when the monochromator is static. The key to detecting dynamics (inelastic neutrons) with the HFBS spectrometer is that the monochromator can oscillate back and forth relative to the incident neutron beam. This Doppler shifts the reflected neutrons; some slightly increase in energy and some slightly decrease. If the frequency and stroke of the Doppler drive oscillation are known, it is possible to calculate the broadened energy distribution of the Doppler-shifted, initially monochromatic neutron beam. However, only those Doppler shifted neutrons that change back to their original incident 6.271 \AA wavelength after scattering are able reflect off of the Debye-Scherrer ring and into the detectors. From this it is possible to determine the energy distribution of the scattered neutrons.

The NIST High Flux BS spectrometer is capable of detecting much smaller neutron energy exchanges with the sample, and therefore slower dynamics than the TOF spectrometer. The incident energy beam can be collimated to $0.85 \mu\text{eV}$ FWHM in terms of an elastic energy resolution. This means that motions faster than 205 MHz can be seen by the HFBS spectrometer; slower motions appear as static. This energy resolution is much closer to the frequencies accessible in through a NMR measurement. In terms of wave numbers, the HFBS is sensitive to modes of 0.007 cm^{-1} and higher in energy. In addition, the maximum energy gain or loss HFBS can detect, the so-called energy window, is defined by the Doppler driver. The energy window of the NCNR HFBS is $\pm 36 \mu\text{eV}$. All scattering events outside of the energy window, associated with fast relaxation processes, appear as background under the scattering spectrum.

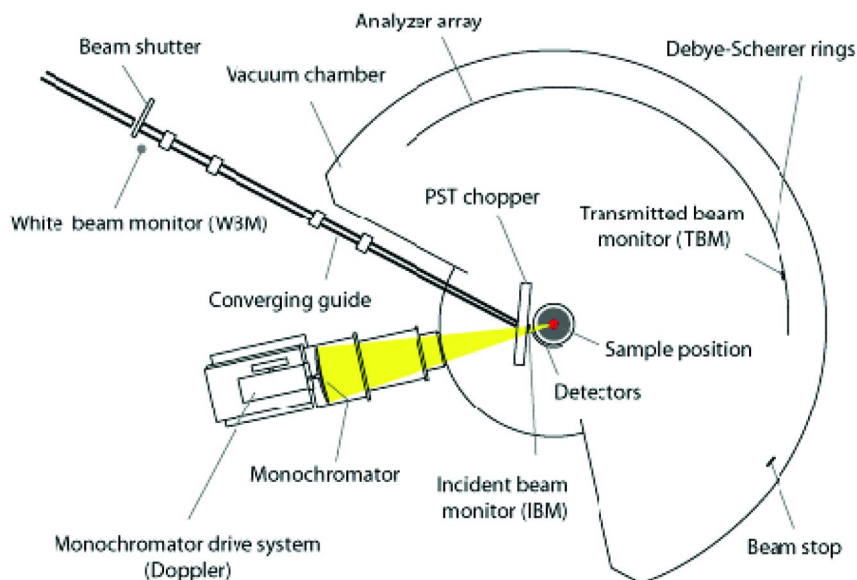


Figure 5. A schematic representation of the High Flux Backscattering Spectrometer available through the NCNR (19). The neutrons fly down the incident guide and converge on the PST chopper which reflects them into the Doppler drive monochromator. This redirects the neutrons back onto the sample where they scatter into the analyzer crystals located on the Debye-Scherrer rings. Only those neutrons with the appropriate energy are reflected back into the detector bank located right behind the sample.

Another INS technique, neutron spin echo (NSE), employs neutron's spin and magnetic moment in a magnetic field. Polarized neutrons are sent through two symmetric magnetic fields before and after the sample. At the sample a π spin flip occurs by a flipper. If the scattering process is strictly elastic the Larmor precession angles in the two fields are equal and opposite, so that full polarization is recovered, irrespective of the initial neutron velocity (energy) distribution. Quasielastic scattering with the sample leads to a change in the neutron energy and one in the precession angle of the outgoing beam, resulting in a decrease in the polarization. Basically, NSE is also time-of-flight technique and it achieves high energy resolution (as small as neV) by encoding the neutron energy into neutron spin Larmor precession angle. With the manipulation of the neutron spin, NSE spectrometers directly measure the real part of the intermediate function $S(Q,t)$ by scanning the magnetic fields in the coils and measuring the polarization. Another important property of NSE is its ability to distinguish coherent from incoherent scattering. The incoherent INS, which alters both the spin and energy of the neutrons, provides only the background or noise in NSE measurement. More details about this instrument can be found on NCNR website (19).

INS Data Interpretation

To understand the nature of the motion in a polymeric or soft organic material, the Q and ω (frequency) dependence of the scattered neutrons must be modeled to extract the characteristic lengths and time scales of the motion. Q is the space Fourier transform of the relevant length scales while ω is the Fourier transform of the time scales of the motion into the frequency (or energy) domain. The Q and ω dependence of the scattered neutrons contain all the spatial and temporal characteristics information of the dynamics that fall within the energy and Q resolution of the spectrometer. It can be challenging to extract the proper details of the motion given inverse problem (loss of phase information) in the scattering process. Therefore, the experimental data must be modeled and inherent assumptions or limitations are often implied by the nature of the model. Most INS measurements in polymeric materials focus on the incoherent neutron scattering given that the incoherent cross-section dominates the scattering for hydrogenous materials and, therefore, provide self correlation function of the hydrogens. A common starting point for most dynamic models is the one-phonon approximation:

$$S_{inc}(Q, \omega) = \frac{3N\hbar}{2M} e^{-2W} Q^2 \frac{n(\omega) + 1}{\omega} g(\omega) \quad (1)$$

where $S_{inc}(Q, \omega)$ is proportional to the number of neutrons (i.e., intensity) scattered at a wave vector Q with a frequency ω , and $g(\omega)$ is the density of states, $n(\omega) + 1$ is the Bose population factor, and e^{-2W} is the Debye-Waller factor. In this expression, $W = (1/6)Q^2\langle u^2 \rangle$, with $\langle u^2 \rangle$ denoting the mean-square atomic displacement. The prefactor $3N\hbar/2M$ contains all the information about the total number of scattering nuclei in the sample and their representative scattering cross sections. The process of choosing an appropriate model for the motion is beyond the scope of this chapter. However, there are several excellent textbooks dedicated to this subject (15, 17, 18). In the following we present a few of the most simple models, but sufficient to illustrate the power of the technique.

Quantitative analysis of the INS spectra from a polymeric material can be challenging since in most cases one is unable to work out an exact model for the scattering function to be compared with the experimental data, as is frequently done, e.g., in molecular crystals. In many instances the polymeric material is disordered or amorphous, as is often the case with polymer electrolytes with a lithium salt complex system. This leads to a broad spectrum of relaxation processes whose characteristic times range from picoseconds to seconds. INS is a microscopic method sensitive to fast local motions in the pico to nano second region. Typically, these are side group rotations or stochastic motions of chain segments. The data fitting and analysis often requires trial and error to achieve fitting results that are *mathematically* acceptable and make *physical* sense. The general equation to model the INS data contains three different terms (17):

$$S_{theo}(Q, \omega) = \text{DWF} \{ A_0(Q)\delta(\omega) + [1 - A_0(Q)]S_{QE}(Q, \omega) \} + \text{BKG} \quad (2)$$

where DWF is the usual Debye Waller factor discussed above, $A_0(Q)$ is the so-called elastic incoherent structure factor (EISF), $\delta(\omega)$ is the Dirac delta function at zero frequency, $S_{QE}(Q,\omega)$ is the quasi-elastic scattering model function and BKG is the background. EISF approaches zero for purely diffusive or diffusive-like processes and the data analysis becomes much simpler. The Delta function in eq.2 accounts for any processes that are slower than the instrumental resolution and the background accounts for faster dynamical processes that are outside the dynamical range of the instrument. Equation 2 should also be convoluted with instrumental resolution before it can be fitted to the measured experimental data; The first commonly used approach is to treat the QE signal, $S_{QE}(Q,\omega)$, by a single Lorentzian function. A Lorentzian function can describe many types of molecular motions such as diffusion and rotation (17). Furthermore, the fourier transform of an exponential decay function, $\exp[-t/\tau]$, is also a Lorentzian function. Thus, a Lorentzian function can be interpreted as pure exponential relaxation process with a single relaxation time τ . However, for the polymer segmental motion, a single Lorentzian is, often, not enough and, usually, a stretched-exponential function or Kohlraush William Watts (KWW) function (22) fits the data well. The KWW function, in the time domain, is given by:

$$\Phi(t) \approx \exp\{-(t/\tau)^\beta\} \quad (3)$$

where τ is the characteristic relaxation time and β ($0 < \beta < 1$) is the stretched exponential parameter defining the non-exponential behaviour of the relaxation. The KWW function has been used to describe the dynamics of amorphous liquids and polymer segmental motions in literature by many researchers. The KWW model can be thought of a distribution of relaxation times and has also been interpreted in heterogeneous and homogeneous scenarios of the molecular dynamics (23). However, fitting the QENS data to KWW function is not free from challenges. As the QENS data is typically available in energy domain (for the TOF and BS spectrometers, but not the NSE spectrometer) and the KWW function has no exact functional form other than $\beta=0.5$ (24), Fourier transform of the KWW function has to be performed before it can be fitted to experimental data. However, such analysis only works if all the other components that contribute to the scattering besides the KWW function are known. For example, if there is an elastic contribution, then the shape parameter β and relaxation time τ will be strongly coupled to the a priori unknown elastic intensity or $A_0(Q)$. On the other hand, one can perform inverse Fourier transform of $S(Q,\omega)$ to obtain $S(Q,t)$ and then fit the data in time domain. Unfortunately, the truncation errors involved in Fourier transform due to the limited frequency range in the experimental data can be overwhelming. In addition, shape parameter and relaxation time are strongly coupled and the correlation matrix has to be examined carefully before analysing the results (25). Fortunately though, in polymer systems the shape parameter β is found to be Q independent which makes the fitting procedure relatively easier as one can fix the shape parameter to average values and determine the relaxation times with better accuracy.

Another form of data obtained from INS measurements, almost entirely HFBS measurements, that is not discussed above is the so-called fixed window scan

(FWS). In FWS, the Doppler driver of the HFBS spectrometer in Figure 5 is held stationary and only the intensity of the elastically scattered neutrons are measured. Dynamic processes and inelastic scattering that are within the energy window of the spectrometer also result in a loss of the elastic scattering intensity. Typical FWS experiments are done by heating or cooling the sample at a certain rate and recording the elastic intensity as a function of Q . As the total scattering (elastic plus inelastic) is conserved, a decrease in the elastic intensity infers an increase in the inelastic intensity. As only the elastic intensities ($\omega = 0$) are considered, the Q dependence of the normalized elastic intensity I_{inc} can be quantified in terms of a Debye-Waller factor approximation (26) where the hydrogen weighted mean-square atomic displacement $\langle u^2 \rangle$ is given by:

$$I_{\text{inc}}(Q,T)/I_{T0}(Q) = \exp\{-Q^2 \langle u^2(T) \rangle / 3\} \quad (4)$$

In the above eq., $I_{T0}(Q)$ is the purely elastic intensity and can usually be measured on a sample at low temperatures, approaching 0 K, where no dynamics are expected on the time scale of backscattering instrument. With this assumption, a plot of $\ln(I_{\text{inc}}/I_{T0})$ versus Q^2 is linear and the slope provides value of the mean square displacement $\langle u^2 \rangle$ at a given temperature. Although most atomic motions in soft condensed matter are admittedly anharmonic, this approximation has been useful for characterizing the dynamics of polymers and other glass formers. In the following sections, we will review some of the literature on the dynamics of polymer electrolytes and learn about some of the progress that has recently been made using INS.

Relaxations in Polymer Electrolytes with Lithium Salt

Although the conduction mechanism of Li^+ ions in polymer electrolytes is not yet fully understood, it is commonly accepted that the hopping rate of the charge transfer is directly influenced by local and segmental motion of the polymer. In order to understand the coupling between the charge transfer and the molecular motions in the polymer electrolytes, it is necessary to understand the polymer relaxation processes. When a lithium salt is solvated by polymers such as poly(ethylene oxide) (PEO), each Li^+ ion is coordinated with several ether oxygen atoms on single or perhaps multiple polymer chains. The Li^+ ion transport in the electrolytes involves re-coordination of the charge with neighboring oxygen-bearing groups. The formation and disruption of these coordination sites must be accompanied by relaxation of the local polymer segments. The main focus of existing measurements is to see how the polymer motion changes upon the addition of the lithium salt. Below we summarize the different attempts by researchers in this field to analyze their INS data on such systems. Most of the data thus far has been obtained on TOF and BS spectrometers, but there have also been a few reports utilizing NSE spectrometers.

Some of the first INS studies on polymer electrolyte system were reported on PPO (polypropylene oxide) and its salt blends (25, 27). In these systems, fixed center of mass methyl group rotations are activated at a lower temperatures than the longer range segmental motion associated with the glass transition; these

methyl group rotations must be considered when fitting the spectra measured at higher temperatures. Carlsson et al accounted for the methyl group rotation using a well-established jump rotational model, after which the segmental motion was described in terms of a stretched exponential relaxation (27). In comparison to neat PPO, the segmental motion of the blend with LiClO₄ (O:Li = 10:1) was found to be slower and moved outside of the experimental time window of the TOF measurements. However, the characteristic times for methyl group rotation were not affected. These results suggest that the coordination of ether oxygen atoms to the Li⁺ ions constrains the segmental motion, but does not affect the methyl group rotation. This is not surprising since the non-polar methyl groups do not interact strongly with the ions and their rotation is fixed center of mass movement; they should not have a strong influence on ion transport. However, since the scattering from the methyl group rotation is very pronounced, it can dominate the spectra; methyl rotation can become a nuisance when trying to analyze INS data for diffusive motions that are more relevant to transport. A much simpler system to work with is PEO and its lithium salt blends, on which the vast majority of the INS measurement have focused on.

The INS spectra of neat PEO can be readily fit with the KWW function. Mao et al have argued that this KWW relaxation in neat PEO is translational in nature (28). In the presence of Li salts, these relaxations show quite a different nature in a way that depends on the type of anions. For the PEO-LiClO₄ system, data was modeled to an elastic peak and a simple Lorentzian function to capture the relaxation process. The FWHM of the Lorentzian for the PEO fast relaxation did not show any Q dependence in the presence of LiClO₄, indicating that the translational motions had become localized. On the other hand, the spectra of PEO blended with LiTFSI (lithium bis(trifluoromethanesulfonyl)imide) required the addition of one more exponential decay process (one more Lorentzian function) to adequately fit the data. These fast single exponential components were attributed to rotational motions stemming from rapid conformational fluctuations of the chain segments between Li coordination sites. These fluctuations were thought to be associated with the making and breaking of the coordination bonds that assist the Li⁺ ion transport in these electrolytes. Mao et al also argued that the appearance of the elastic component in PEO complexed with the Li salts reflected a slowing down of the translational motion of the chain segments. Both NSE measurements and molecular dynamics simulation support this notion (29, 30). The intermediate scattering function from the NSE measurements show that adding salt increases the polymer relaxation times by 2-3 orders of magnitude, accompanied by a decrease in the stretching parameters by a factor of 2-3; this suggests a broader distribution of characteristic time scales. In a related study by Triolo et al, a combination of a KWW function for the segmental motion and a Lorentzian function for librational modes was used to model the TOF data of pure PEO (31). For the dynamics of PEO with lithium salt, Triolo et al found that a slower relaxation process was needed to fit the data and they attributed this additional process to the segmental dynamics of the restricted PEO chains involved in Li⁺ ion coordination. In general the notion that the addition of Li⁺ ions that interact with multiple ether oxygen segments leads to retarded dynamics of the PEO and increased elastic scattering seems very reasonable.

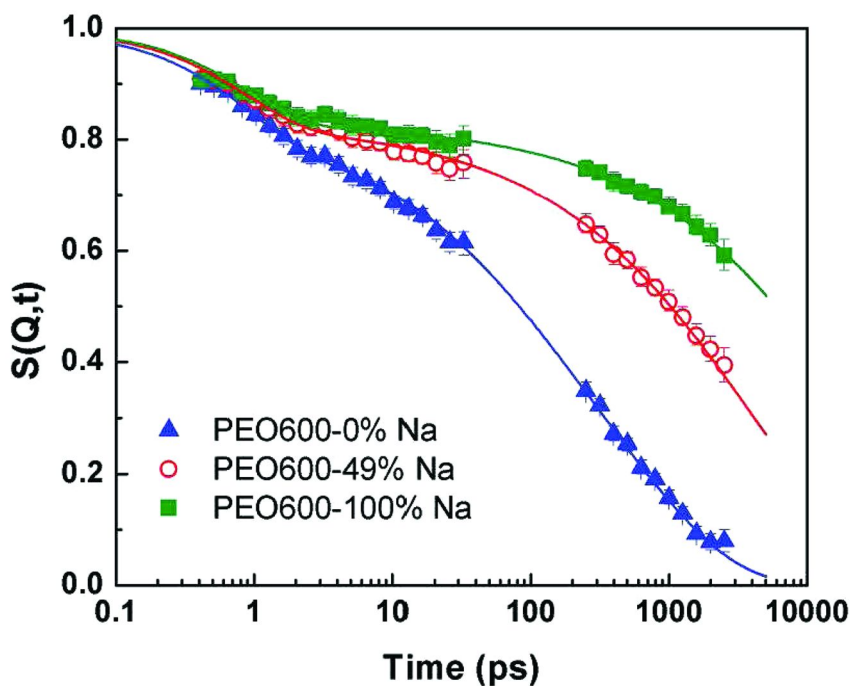


Figure 6. Intermediate scattering function, $S(Q,t)$, for three polyester single ion conductors (33). The percentage number indicates the degree of the isophthalate groups that were substituted with sodium sulfonate. The data symbols are derived from Fourier transform of the TOF (less than 100 ps) and of HFBS (beyond 100 ps) INS data. The lines are fits to the sum of two KWW functions.

Fullerton-Shirey et al studied the dynamics of PEO in its neat form and in blends with LiClO_4 for varying ratios of O:Li using both the TOF and BS spectrometers (32). In their approach, the intermediate scattering functions, $S(Q,t)$, were obtained via a frequency domain Fourier transform of the reduced $S(Q,\omega)$ data. Two KWW functions were found to be necessary to fit the combined QENS data covering a time span from 0.4 ps to 2.5 ns. The faster KWW process, with Q dependent relaxation times was attributed to the segmental mobility of PEO while the slower KWW process, with Q independent relaxation time was attributed to of the restricted rotation of protons around the Li^+ ions. Assuming that the ether oxygen atoms on PEO chains coordinate with Li^+ ions, they proposed a rotational model with non-uniform distribution. The most surprising result of this study was that the segmental mobility of PEO chains was found to decouple from the ionic conductivity. As these measurements were only sensitive to the local motions in the amorphous phase, Fullerton et al interpreted this decoupling as the consequence of ion conduction through the crystalline phase only. This is intriguing as ion transport is largely believed to be limited to the amorphous regions. In continuation, Sinha et al measured PEO electrolytes with a polyester single ion conductor (33). The polyester single ion conductor was

composed of PEO spacers, separated by isophthalate groups, with varying degrees to which a sodium sulfonate group was attached. The combined intermediate scattering function again required two KWW processes (as shown in Figure 6) to fit the experimental data. The faster process was attributed to the PEO units away from the ions; the dynamic features of this process were very similar to the segmental motion observed in neat PEO and its lithium salt blends discussed above. The slower process appeared to be related to the PEO units close to the ions. The significant increase in the relaxation time of the slow process with the increase of ion content was explained in terms of ionic cluster formation.

Fixed window scan (FWS) are also used to study the dynamics of polymer electrolytes for battery applications. Later in this manuscript we will discuss some of our own traditional FWS measurements on hyperbranched PEO molecules that inhibit crystallization. In a unique backscattering spectrometer, Russina et al used a monochromator made of $\langle 111 \rangle$ oriented $\text{Si}_{0.9}\text{Ge}_{0.1}$ crystals, instead of the conventional $\langle 111 \rangle$ Si crystals that are used in typical backscattering spectrometers (34). The lattice spacing of the their monochromator was slightly different from that of the conventional $\langle 111 \rangle$ Si analyzer by an amount that corresponds to an energy transfer of $-14.5 \mu\text{eV}$. With the modified analyzer the FWS measurements only detect neutrons that are scattered inelastically with an energy of $-14.5 \mu\text{eV}$; this measurement is more appropriately referred to as an inelastic fixed window (IFW) scan. Russina et al measured both neat and LiTFSI doped PEO-PPO random copolymer using this technique. The IFW data were modeled with a Cole-Davidson (CD) type susceptibility for the relaxation process and the relaxation times were assumed to follow the usual Vogel-Fulcher-Tammann (VFT) type temperature dependence. In agreement with previous results, Russina et al found that the methyl group dynamics were unaffected by the salt addition. However, they discovered that the segmental motions of the salt blend were bimodal, including a faster process that is identical to the relaxation process in the neat polymer and the slower one corresponding to the relaxation of the polymer segments involved in the Li^+ ion complexation (see Figure 7).

Dynamics in Nanocomposite Polymer Electrolytes

The influence of nano-composites on the ionic conductivity of a polymer electrolyte was first reported in the seminal work of Croce et al (35). They reported that the addition of inorganic nanoparticles such as Al_2O_3 and TiO_2 can increase the polymer electrolyte conductivity several fold, both below and above the PEO melting temperature. The increased conductivity below the PEO melting temperature might be understood by the nanoparticles reducing the crystallinity of the PEO. However, the ten-fold increase in conductivity above the PEO melting temperature appeared to suggest that the charge transport mechanism or the polymer dynamics were fundamentally modified. This spurred significant interest, both experimentally and theoretically, to uncover the mechanism behind the increased ion conductivity. Fullerton-Shirey et al employed INS measurements to quantify the dynamics of the PEO electrolytes both with and

without Al₂O₃ nanoparticles (36). These measurements suggested that both the PEO segmental motions and the rotational motion of the Li coordination sites that they had previously reported (32) were unaltered by the presence of nano-fillers. The only exception was that the rotation modes became slightly restricted at a concentration where O:Li ratio was 8:1. However, unlike the Croce et al., their measurements generally did not show improved ion conductivity upon adding Al₂O₃ nanoparticles. The only exception was when the O:Li ratio was 10:1, a specific loading that corresponds to an eutectic concentration. In agreement with their previous work (32), the increased conductivity could not be associated with enhanced polymer dynamics and the two were found to be decoupled.

In order to discriminate between the effect of nanoparticles on crystallinity and other confinement effects, such as changes in segmental mobility as discussed above, Karlsson et al used QENS to investigate a system based on a completely amorphous polymer trihydroxy poly(ethylene oxide-co-propylene oxide) (3PEG) (37). In this study, the diffusive segmental motions of the bulk polymer, the methyl group rotation, and fast local chain motions were modeled by several Lorentzian functions, while an elastic component was added to account for the slow relaxations (not in the window of the spectrometer) of immobilized chain segments. These measurements showed that the elastic peak increased in intensity upon the addition of TiO₂ nano-fillers. Karlsson et al proposed that there was an immobilized layer of polymer surrounding the nano-fillers. They calculated the thickness of this layer to be approximately 4-5 nm, thereby accounting for about 5% of the total polymer volume. Interestingly, the fast processes remained unchanged in all samples, suggesting polymer dynamics did not contribute to the increased ion conductivity in the nanocomposite polymer electrolytes.

In all the studies discussed thus far, the information of the ionic motions have been deduced indirectly by analyzing the dynamics of the polymer electrolyte as the Li⁺ ions themselves do not have appreciable neutron scattering cross section; they do not contribute significantly to the observed neutron scattering intensity. Eijck et al performed interesting INS experiments on the mixture of deuterated PEO oligomer and NH₄I, both with and without TiO₂ nanoparticles (38). The purpose of these experiments was to make the PEO oligomer molecules practically invisible in QENS measurements so that the cation dynamics could be observed directly. Interestingly, the QENS spectra showed a significant increase of the quasi-elastic scattering intensity in the nanocomposite polymer electrolyte. Van Eijck et al proposed that the addition of nano-fillers increased the population of mobile NH₄⁺ cations which also resulted in the enhanced ion conductivity. Although an extension of these results, obtained from a model cation system, cannot be directly made to the Li⁺ ion PEO systems, the results are entirely consistent with the observed increase in conductivity upon the addition of nanoparticles. The increased conductivity of polymer electrolytes upon the addition of nanoparticles could be due to reduced interaction strength between the ether-oxygen and the cations, rather than the increase in polymer dynamics. This notion is also in agreement with the conclusions of Karlsson et al (37).

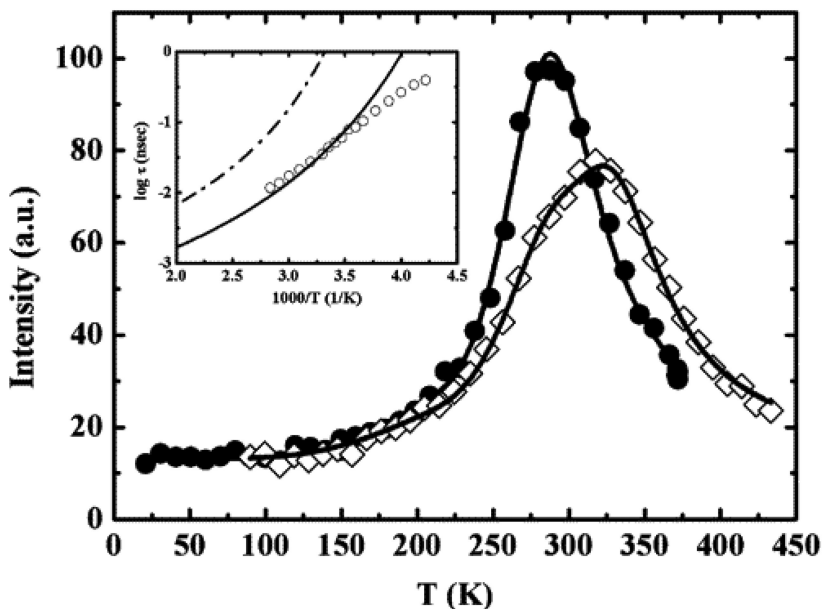


Figure 7. Comparison between the inelastic fixed window energy scans on the neat (filled circles) and lithium salt doped (open diamonds) PEO-PPO random block copolymer (34).

Relationship between Fast Segmental Motion and Ion Transport

In most of the examples discussed thus far, the focus has been on relating the quasielastic or inelastic scattering that describes the relaxation processes in the polymer to the ion conductivity. This requires fitting the scattering data with the appropriate relaxation models that describe the motion. For complicated motions, this fitting can be very complicated as the number of processes and fitting parameters increases. In the field of polymers, biological materials, and soft matter, it has also been realized that the temperature and Q dependence of the elastic scattering, which is trivial to characterize, can provide a very meaningful approximation for the polymer dynamics with very few fitting parameters (39). This analysis is based on the Debye-Waller approximation presented in Equation 4. The elastic scattering experiment that measures mean square displacement of a system, also provides a simplified but direct measure of the molecular mobility. As an example, a correlation between viscosity and the atomic mean-square displacement was first proposed by Buchenau and Zorn (40). For this purpose, the authors defined, $\langle u_2 \rangle_{loc}$, as the difference between the mean-square displacement of the disordered phase (amorphous and liquid) and the ordered phase (crystalline):

$$\langle u^2 \rangle_{\text{loc}} = \langle u^2 \rangle_{\text{disord}} - \langle u^2 \rangle_{\text{ord}} \quad (5)$$

The inverse of the newly defined $\langle u^2 \rangle_{\text{loc}}$ which measures only the part of the mean-square displacement that corresponds to localized modes in the disordered phase, shows a linear relationship with logarithm of viscosity. The above relationship, which was reported for selenium and polybutadiene, can be generalized to amorphous liquids and solids by defining $\langle u^2 \rangle_{\text{loc}} = \langle u^2 \rangle_{\text{liq}} + \langle u^2 \rangle_{\text{hard}}$ where $\langle u^2 \rangle_{\text{liq}}$ is the mean-square displacement for motion faster than the instrumental resolution and $\langle u^2 \rangle_{\text{hard}}$ takes into account only the typical lattice vibrational frequencies. According to the Nernst-Einstein relation, the ion conductivity should be directly related to the viscosity. Therefore, atomic mean square displacements can provide useful insight of the ion conductivity as they seem to be related.

One of the biggest problems in using PEO as a polymer electrolyte is that it crystallizes below 50° - 60°C. This significantly lowers the room temperature conductivity as the ion transport is largely limited to amorphous phase of the semi-crystalline morphology. As mentioned previously, there have been several strategies to suppress crystallization of PEO and improve conductivity at room temperature (3, 5, 8–13). Hyperbranching of a polymer chain is one effective way to suppress crystallization. To better understand the effects of fast polymer dynamics on the ion transport, we studied a series of hyperbranched PEO (hbPEO) with varying degrees of branching, both with and without lithium salts (41). As expected, the hyperbranching suppressed the crystallization and the salt containing samples were found to be amorphous above 0° C, confirmed with differential scanning calorimetry. The temperature dependence of ionic conductivity for different hbPEOs and linear PEO with the lithium salt, LiTFSI, are shown in Figure 8. The Li⁺ ion conductivity showed strong variations with the glycidol (G) branching comonomer content. We investigated hyperbranched PEO copolymers with 8, 16, and 50% glycidol, denoted as hbPEO-G8, hbPEO-G16, and hbPEO-G50, respectively. The hbPEO-G8 displayed the highest conductivity at room temperature and there was a very small decrease in conductivity when moving from 8% to 16% glycidol content, followed by a more significant drop at 50% glycidol (see Fig. 8). The decrease in conductivity at higher glycidol fractions probably reflects the increase in the hydroxyl content with the introduction of the glycidol branching moieties. For each glycidol unit of the copolymer, exactly one additional hydroxyl group is introduced, leading to the formation of a hydrogen-bonded network with increased branching. This was consistent with the visual observation that the room temperature viscosity increases from a viscous liquid that readily flows for hbPEO-G8 to an elastomer-like gel for the hbPEO-G50 sample. In breaking up this hydrogen-bonded network, we also investigated a permethylated version of the hbPEO-G16 where the –OH groups were replaced with –OCD₃ to break up the hydrogen bonds between the polymer termini. The methyl group was deuterium substituted to eliminate the contribution from methyl rotors in the

neutron scattering. As expected, the permethylated sample shows a significant increase in the Li-ion conductivity as shown in Figure 8.

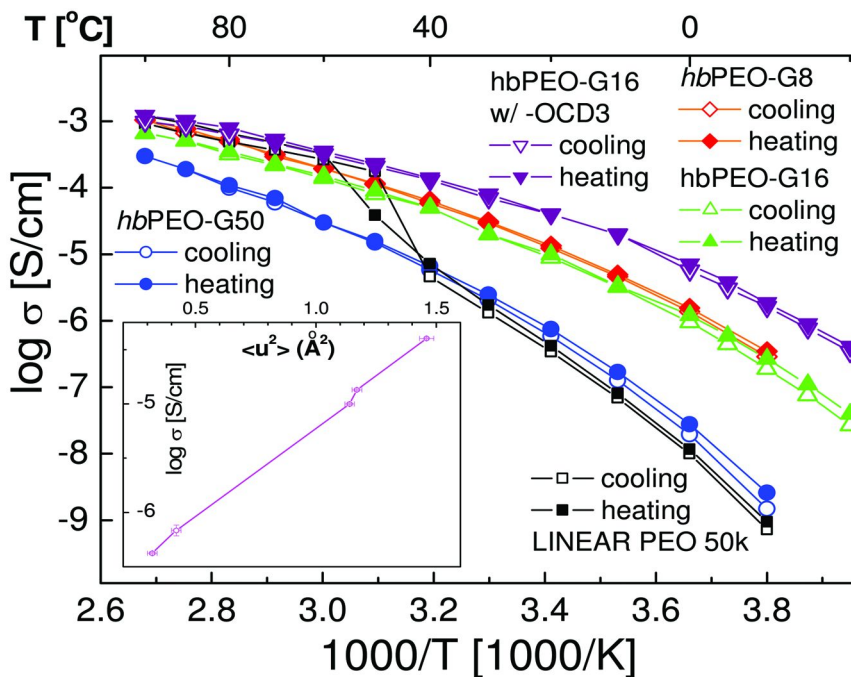


Figure 8. Temperature-dependent Li⁺ ion conductivity for hbPEO samples with varying glycidol branching contents and permethylation, as compared with linear PEO, blended with LiTFSI salt in molar ratio O:Li of 25:1.13 The inset shows a direct correlation between the Li⁺ ion conductivity and the hydrogen weighted mean-square displacement $\langle u^2 \rangle$ as measured by INS at ambient temperature. Figure reproduced from reference (41).

The atomic mean square displacement was obtained from FWS measurements on the HFBS at the NIST Center for Neutron Research, as described in the INS data interpretation section. The inset of Figure 8 shows a well defined relationship between $\langle u^2 \rangle$ and the logarithm of conductivity. This is analogous (but admittedly not identical to) the studies of Buchanea and Zorn that showed an exponential relationship between viscosity and $1/\langle u^2 \rangle$. It is, however, of particular significance that there is a direct correlation between the high frequency segmental dynamics of hbPEOs blended with Li salts probed by the INS measurements and the slower motions of the Li⁺ ions in these polymers. It is generally believed that the Li⁺ ions move through PEO by the Grotthuss hopping mechanism (42) from one association site to the next, involving a catch-and-release process of Li⁺ ions association/dissociation by the PEO segments. The Grotthuss mechanism is then strongly coupled to the segmental reorganization dynamics of the polymer involving the Li⁺ ions. These findings

suggest that the transport of Li^+ ions is closely coupled to the pico- to nanosecond dynamics of polymer chains. The implication is that one should be able to increase the Li^+ ion conductivity of polymer electrolytes by enabling faster local dynamics, as demonstrated here with hbPEO-G16-OC3.

Summary

In this chapter we have introduced the use of INS techniques as a quantitative tool to better understand the mechanisms of Li^+ ion transport through polymeric electrolyte media. We have introduced the concept of inelastic neutron scattering and provided a basic understanding of the types of motions and atomic species to which it is sensitive. We have also provided a brief background on the different types of INS spectrometers that can be used to study the dynamics of different polymers used as electrolytes. The case has been made that the INS measurements of the dynamics in the polymers provide very complimentary measurements to e.g. dielectric measurements that directly quantify ion mobility. Quantifying the dynamics of both the ionic species and the host transport media are important for understanding this complicated transport problem. In particular, we introduced results from the literature indicating that the dynamics of a polymer electrolyte are impacted upon the addition of a Li salt. Typically the segmental or translational relaxations slow down while fixed center of mass motions involving non-polar or non-solvating groups such as methyl rotations are unaffected by the presence of the ions. This generally supports the notion Li^+ ions aggregating with multiple polymer chains in a way that can slow down the molecular and ionic mobility of the entire system; the Li^+ ions act as transient cross-links. The literature reported herein, with a few exceptions, also appears to support a general correlation between the level of molecular mobility within the polymer electrolytes and the ionic conductivity through the electrolyte media. These polymers with enhanced anharmonic or translational relaxation process in the presence of the Li salts also appear to possess increased ionic conductivity. Unfortunately though, polymer dynamics alone were unable to fully explain some of the empirical observations of enhanced conductivity in polymer electrolytes upon the addition of nanoparticle fillers. This underscores the importance of understanding the role of all the interactions between the mobile ions, their counter ions, the polymer electrolyte, and any additional additives is important. In general though, a positive correlation between ion conductivity and viscosity/mobility on the macroscopic scale makes intuitive sense through empirical relations like the Nernst-Einstein equation. The utility of inelastic neutron scattering is that one can focus on the detailed mechanisms at the nanosecond and picosecond time scale to better understand how molecular mobility translates to ion motion. This should provide better insight for understanding ion conductivity in complicated systems and molecular design cues for designing higher mobility solid polymer electrolytes.

References

1. Wakihara, M.; Yamamoto, O. *Lithium Ion Batteris*; Kodansha Ltd.: Tokyo; Wiley-VCH: Weinheim, 1998.
2. Agrawal, R. C.; Pandey, G. P. *J. Phys. D: Appl. Phys.* **2008**, *41*, 223001.
3. Gray, F. M. *Polymer Electrolytes*; Materials Monographs; Royal Society of Chemistry: Cambridge, 1997.
4. Armand, M. B. *Annu. Rev. Mater. Sci.* **1986**, *16*, 245.
5. MacCallum, J. R.; Vincent, C. A. *Polymer Electrolyte Reviews 1*; Elsevier Applied Science: 1987.
6. Meyer, W. H. *Adv. Mater.* **1998**, *10*, 439.
7. Murata, K.; Izuchi, S.; Yoshihisa, Y. *Electrochim. Acta* **2000**, *45*, 1501.
8. Allcock, H. R.; O'Connor, S. J. M.; Olmeijer, D. L.; Napierala, M. E.; Cameron, C. G. *Macromolecules* **1996**, *29*, 7544.
9. Hooper, R.; Lyons, L. J.; Mapes, M. K.; Schumacher, D.; Moline, D. A.; West, R. *Macromolecules* **2001**, *34*, 931.
10. Abraham, K. M.; Choe, H. S.; Pasquariello, D. M. *Electrochim. Acta* **1998**, *43*, 2399.
11. Nishimoto, A.; Agehara, K.; Furuya, N.; Watanabe, T.; Watanabe, M. *Macromolecules* **1999**, *32*, 1541.
12. Hawker, C. J.; Chu, F.; Pomery, P. J.; Hill, D. J. T. *Macromolecules* **1996**, *29*, 3831.
13. Marzantowicz, M.; Dygas, J. R.; Krok, F.; Tomaszewska, A.; Florjanczyk, Z.; Zygado-Monikowska, E.; Lapienis, G. *J. Power Sources* **2009**, *194*, 51.
14. Briant, J. L.; Farrington, G. C. *J. Solid State Chemistry* **1980**, *33*, 385–390.
15. Higgins, J. S.; Benoît, H. C. *Polymers and Neutron Scattering*; Oxford, 1994.
16. Frick, B.; Richter, D. *Science* **1995**, *267*, 1939.
17. Bee, M. *Quasi-elastic Neutron Scattering*; Adam Hilger: Bristol, 1988.
18. Roe, R. J. *Methods of X-Ray and Neutron Scattering in Polymer Science*; Oxford University Press: New York, 2000.
19. <http://www.ncnr.nist.gov>.
20. Copley, J. R. D.; Cook, J. C. *Chem. Phys.* **2003**, *292*, 477.
21. Meyer, A.; Dimeo, R. M.; Gehring, P. M.; Neumann, D. A. *Rev. Sci. Instrum.* **2003**, *74*, 2759.
22. Williams, G.; Watts, D. C. *Trans. Faraday Soc.* **1970**, *66*, 80.
23. Arbe, A.; Colmenero, J.; Monkenbusch, M.; Richter, D. *Phys. Rev. Lett.* **1998**, *81*, 590.
24. Rajagopal, A. K.; Ngai, K. L. *Relaxations in Complex Systems*; North Holland, Amsterdam, 1991.
25. Zajac, W.; Gabrys, B. J.; McGreevy, R.; Mattssons, B. *Physica B* **1996**, *226*, 144.
26. Zorn, R. *Nucl. Instrum. Methods Phys. Res.* **2007**, *572*, 874.
27. Carlsson, P.; Mattsson, B.; Swenson, J.; Torell, L. M.; Kall, M.; Borjesson, L.; McGreevy, R.; Mortensen, K.; Gabrys, B. *Solid State Ionics* **1998**, *113–115*, 139.
28. Mao, G.; Perea, R. F.; Howells, W. S.; Price, D. L.; Saboungi, M.-L. *Nature* **2000**, *405*, 163.

29. Saboungi, M.-L.; Price, D. L.; Mao, G.; Fernandez-Perea, R.; Borodin, O.; Smith, G. D.; Armand, M.; Howells, W. S. *Solid State Ionics* **2002**, *147*, 225.
30. Mos, B.; Verkerk, P.; Pouget, S.; Zon, A. V.; Bel, G. J.; de Leeuw, S. W.; Eisenbach, C. D. *J. Chem. Phys.* **2000**, *113*, 4–7.
31. Triolo, A.; Celso, F. Lo; Passerini, S.; Arrighi, V.; Lechner, R. E.; Frick, B.; Triolo, R. *Appl. Phys. A* **2002**, *74*, S493.
32. Fullerton-Shirey, S. K.; Maranas, J. *Macromolecules* **2009**, *42*, 2142.
33. Sinha, K.; Maranas, J. K. *Macromolecules* **2011**, *44*, 5381.
34. Russina, O.; Triolo, A.; Aihara, Y.; Telling, M. T. F.; Grimm, H. *Macromolecules* **2004**, *37*, 8653.
35. Croce, F.; Appetecchi, B.; Persi, L.; Scrosati, B. *Nature* **1998**, *394*, 456.
36. Fullerton-Shirey, S. K.; Maranas, J. K. *J. Phys. Chem. C* **2010**, *114*, 9196.
37. Karlsson, C.; Best, A. S.; Swenson, J.; Howells, W. S.; Borjesson, L. *J. Chem. Phys.* **2003**, *118*, 4206.
38. Eijck, L.; Best, A. S.; Stride, J.; Kearley, G. *J. Chem. Phys.* **2005**, *317*, 282.
39. Zaccai, G. *Science* **2000**, *288*, 5471.
40. Buchenau, U.; Zorn, R. *Europhys. Lett.* **1992**, *18*, 523.
41. Lee, S.-I.; Schomer, M.; Peng, H.; Page, K. A.; Wilms, D.; Frey, H.; Soles, C. L.; Yoon, D. Y. *Chem. Mater.* **2011**, *23*, 2685.
42. de Grotthuss, C. J. T. *Ann. Chim.* **1806**, *58*, 54.